Epsilon-near-zero nanoparticles

Ibrahim Issah ⓘ, Jesse Pietila ⓘ, and Tommi Kujala ⓘ
Faculty of Engineering and Natural Sciences, Tampere University, 33720 Tampere, Finland

Matias Koivurova ⓘ
Tampere Institute for Advanced Study, Tampere University, 33100 Tampere, Finland
and Faculty of Engineering and Natural Sciences, Tampere University, 33720 Tampere, Finland

Humeyra Caglayan ⓘ[*] and Marco Ornigotti ⓘ[†]
Faculty of Engineering and Natural Sciences, Tampere University, 33720 Tampere, Finland

In this work we propose epsilon-near-zero (ENZ) nanoparticles formed of metal and dielectric bilayers and employ the effective-medium approach for multilayered nanospheres to study their optical response. We obtain a passive tunable ENZ region by varying the radii of the proposed bilayer nanospheres, ranging from visible to near IR. In addition, we present the absorption and scattering cross section of ENZ nanoparticles using open-source transfer-matrix-based software (STRATIFY). The proposed ENZ nanoparticle is envisioned to be experimentally realized using chemical synthesis techniques.

I. INTRODUCTION

Epsilon-near-zero (ENZ) materials exhibit a dielectric permittivity approaching zero at a frequency close to the material's plasma frequency [1,2]. Transparent conductive oxides such as indium tin oxide are naturally occurring ENZ materials with ENZ wavelengths in near-infrared and midinfrared regions [3]. A metamaterial composed of alternating layers of metal and a dielectric was also demonstrated to exhibit ENZ properties in the visible region [4,5].

Notably, ENZ materials studied by many authors consist of nanostructures or meta-atoms, which require fabrication techniques such as focused ion beam milling, laser ablation, atomic layer deposition, and electron-beam lithography [6,7]. On the other hand, the synthesis of nanoparticles and their incorporation into materials are among the most studied topics in chemistry, physics, and material science. Furthermore, it has been demonstrated that localized surface plasmon resonance (LSPR) depends on the size, shape, and material of the nanoparticles. For example, small Au nanoparticles (between 5 and 10 nm) have the LSPR band around 520 nm, while for bigger particles (between 50 and 100 nm), this peak is redshifted up to 570 nm. Other materials such as transparent conductive oxides, transition metal nitrides [8], organic conductive materials [9], and highly doped semiconductors have also been identified to exhibit plasmonic behavior at different spectral regions. In addition, nanoparticles composed of a metal-dielectric complex have been shown to exhibit interesting light-matter interactions with many vital applications in physics and chemistry, such as scattering [10,11] and nonlinear optics [12,13], sensing [14,15], fluorescence [16,17], and up-conversion enhancement [18], surface plasmon amplification [19,20], hydrogen generation [21], and solar energy harvesting [22,23].

Although planar films made of similar materials have been investigated as an ENZ medium for many applications, nanoparticles have not been considered ENZ materials. We envision that the ENZ nanoparticles could provide a new design solution for low-cost tunable ENZ materials, which have wide prospects for application in photonics.

In this work we propose the possibility of the utilization of nanoparticles as ENZ materials. To verify this approach, we employ the effective-medium approach to model the optical response of a multilayer sphere as an effective bulk spherical medium. In particular, by varying the structural properties of the nanospheres, we show how the ENZ character of such multilayered nanoparticles can be easily tuned from the visible to the near-IR region of the electromagnetic spectrum.

II. STRUCTURE DESIGN AND MODELING

The ENZ nanoparticles we consider in this work are bilayer structures consisting of an inner dielectric core, for which we employ SiO_2, and an outer metallic shell, as shown schematically in Fig. 1. Due to the high carrier concentration, electron mobility, and strong electromagnetic-field confinement property of noble metals [24], we choose silver for the outer shell.

To analyze the absorption and scattering of the aforementioned ENZ nanoparticles, we use a transfer-matrix approach (based on the open-source STRATIFY code [25]). As a sanity check, we also implement the optical response (i.e., scattering

[*]humeyra.caglayan@tuni.fi
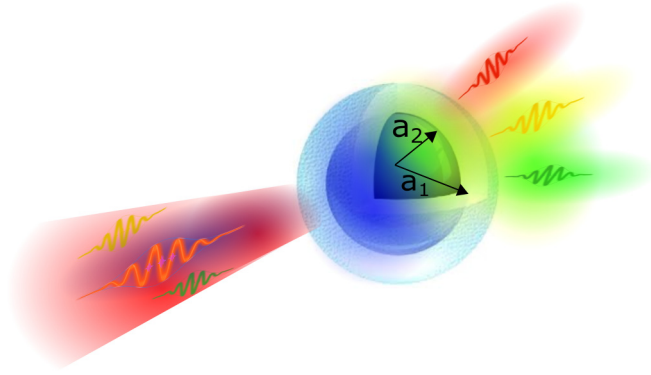[†]marco.ornigotti@tuni.fi

FIG. 1. Schematic representation of the bilayer spherical nanoparticles. Here a_2 and a_1 represent the inner and outer radii of the sphere. The inner, dark blue, sphere represents the dielectric core (SiO$_2$) of the nanoparticle, while the outer, light blue, shell represents the silver coating.

and absorption) for different materials and identify that the Ag-SiO$_2$ bilayer structure gives us the required ENZ region of interest (i.e., visible to near IR). First, we focus on the effective ENZ optical responses of a bilayer spherical nanoparticle embedded within a host medium (i.e., air) and later extend the effective permittivity approach to multilayer nanosphere composites.

The wavelength-dependent complex dielectric functions for Ag and SiO$_2$ are taken from the material data of Johnson and Christy [26]. The scattering, absorption, and electromagnetic near-field distribution are calculated using STRATIFY (i.e., recursive transfer-matrix method MATLAB code).

III. THEORY

In this section we briefly present the theoretical background needed to derive the effective permittivity of the bilayer spherical nanoparticle. Our approach makes use of an effective description of the electric permittivity of a metal-dielectric layered nanoparticle, following the methods presented in Ref. [27]. Although there are many different analytical methods available in the literature to describe the interaction of electromagnetic waves with layered media, such as dyadic Green's functions [28] or vector spherical harmonics decomposition in layered media [29], we choose to use the effective-medium approximation for its unique ability to assign a single effective permittivity to the multilayered nanoparticles. This method has been successfully applied in the past to effectively describe the properties of hyperbolic metamaterials [30,31] in an easy-to-engineer manner. Inspired by this, we decided to use the effective-medium approximation to provide easy-to-engineer ENZ properties of layered nanoparticles. To start with, we assume that a bilayer (and, by simple generalization, a multilayer) nanoparticle can be seen as a composite material, where the outer layer (the shell) plays the role of the host medium, whereas the inner layer (the core) is the inclusion. This assumption allows us to use the theory of effective media to simplify the complex problem of a multilayered spherical nanoparticle, reducing it to the simpler one of a single homogeneous spherical nanoparticle, described via an effective permittivity.

For the case of a metal-dielectric nanoparticle like the one depicted in Fig. 1, for example, this can be easily done using standard methods of electrostatics, i.e., by placing the nanoparticle in a homogeneous electric field and solving the Laplace equation for the electrostatic potential in the whole space [32]. By using this procedure, one can easily show that the electric field generated by the bilayered sphere in the host medium (air, in the case of Fig. 1) is the same as that of a single sphere with radius a_1 and permittivity

$$\tilde{\epsilon}_1 = \frac{1 - 2G}{1 + G}\epsilon_1, \tag{1}$$

with

$$G = \frac{\epsilon_1 - \epsilon_2}{2\epsilon_1 + \epsilon_2}\left(\frac{a_2}{a_1}\right)^3, \tag{2}$$

with ϵ_1 the permittivity of the shell, ϵ_2 the permittivity of the core, and a_2 the radius of the inner sphere.

The above theory can then be generalized for multilayered structures by expressing the multilayered permittivities by simply applying Eq. (1) recursively to each couple of layers, from the outer to the inner one [27], thus obtaining, for the general kth layer,

$$\tilde{\epsilon}_k = \frac{1 - 2G_k}{1 + G_k}\epsilon_k, \tag{3}$$

with

$$G_k = \frac{\epsilon_k - \tilde{\epsilon}_{k+1}}{2\epsilon_k + \tilde{\epsilon}_{k+1}}\left(\frac{a_{k+1}}{a_k}\right)^3. \tag{4}$$

Here the layers are numbered from outside to inside so that $k = 1$ represents the outer layer and $k = N$ represents the inner one. The permittivity for each layer $k = \{N - 1, N - 2, \dots, 2, 1\}$ is expressed using the above equations.

IV. RESULTS AND DISCUSSION

From the above theory, we determined the effective permittivity for the proposed spherical bilayer structure to obtain the ENZ points as a function of the varied core diameters with outer layer thicknesses fixed at 2 nm. Figure 2 shows the effective permittivities for the different ENZ nanoparticles with different core diameters (i.e., $a_{2,1} = \{38, 40\}$, $a_{2,1} = \{68, 70\}$, and $a_{2,1} = \{98, 100\}$ nm). Here $a_{2,1}$ represents the radii of the inner and outer shells, respectively. We obtained different ENZ points by changing the radii of the bilayer nanospheres.

In particular, for $a_{2,1} = \{38, 40\}$ nm [Fig. 2(a)], the ENZ wavelength is found to be $\lambda_{\text{ENZ}} \approx 659$ nm. Similarly, by changing the inner and outer radii of the ENZ nanoparticle, we observe a redshift of the ENZ wavelength to $\lambda_{\text{ENZ}} \approx 852$ nm [Fig. 2(b)] and $\lambda_{\text{ENZ}} \approx 1010$ nm [Fig. 2(c)], respectively. This is the first main result of our work which extends to the numerical calculations of the nanosphere's near-field enhancement, absorption, and scattering cross sections as well as exploiting the possibility of using the effective-medium formulations of bilayer nanospheres into multilayer ENZ nanoparticles.

Ag-SiO$_2$ nanoparticles clearly show ENZ behavior in the visible and near-IR spectral regimes. The position of the ENZ wavelength of such nanoparticles can be easily controlled by suitably tuning the inner core of the nanoparticle. In our
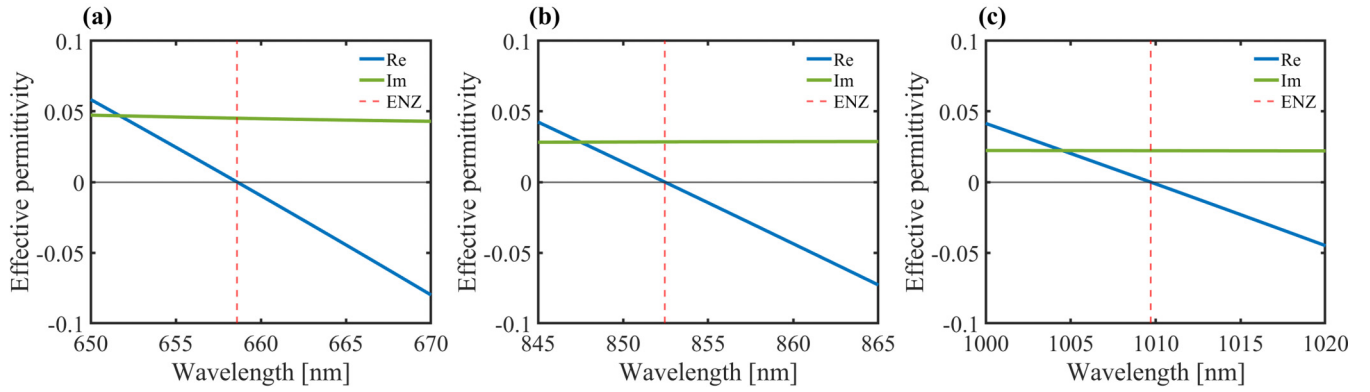
FIG. 2. Effective permittivities of different bilayer spheres near their characteristic ENZ wavelengths (a) $a_{2,1} = \{38, 40\}$, (b) $a_{2,1} = \{68, 70\}$, and (c) $a_{2,1} = \{98, 100\}$ nm. Here Re and Im represent the real and imaginary parts of effective permittivity, respectively. Their corresponding ENZ wavelengths are marked with red dashed lines.

simulations, it was found that the outer radius of the Ag-SiO$_2$ nanoparticle should fulfill $a_1 \leqslant \lambda_{\text{ENZ}}/10$. This is compatible with the implicit assumption, used to derive our effective model, that the wavelength of the electric field should be much larger than any length scale in the system, to guarantee that the effective-medium approach remains valid (i.e., it makes sense to use the Laplace equation for the electrostatic potential near a multilayered sphere to calculate the effective permittivity of such structures).

In addition, it was identified that one should consider the parametric variations of the inner core and outer shell of the nanoparticles, as huge thickness variations between the two layers could affect the bilayer nanoparticle from exhibiting ENZ properties. This is due to the bilayer nanoparticle exhibiting properties of the outer shell instead of the complex media. As such, it is relevant to choose the right fill fraction of the nanoparticle to attain the required ENZ properties.

To verify the reliability of the effective-medium approach described above, we compare the electromagnetic-field distribution of the proposed effective-medium theory and the bilayer structure. As can be seen from Fig. 3, the electric-field distributions outside the nanoparticle, calculated using STRATIFY, for both the case of a bilayer structure [Fig. 3(a)] and a bulk sphere with effective permittivity ϵ_{eff} [Fig. 3(b)]

at the ENZ wavelength, give relatively similar results, as can be seen from Fig. 3(c). The origin of this discrepancy can be traced back to the presence, in the actual bilayer structures, of surface waves, due to the external metallic coating, which locally modifies the electric field of the nanoparticle, making its near field different from the case of the effective medium. From this perspective, therefore, the fact that we observe, as reported in Fig. 3(c), the difference in the very vicinity of the surface of the nanoparticle is quite small, which is somehow expected, and does not jeopardize the validity of the effective-medium approach. This effect has been observed in similar situations, in planar metal-dielectric-based metamaterials [33]. Moreover, we also identified that a bilayer metal-dielectric structure is sufficient to obtain the desired ENZ properties. As a result, we focused on the particle with radii $a_{2,1} = \{98, 100\}$ nm, which can produce Rayleigh scattering since the particle size is smaller than the wavelength of the impinging electromagnetic field. Although a full numerical optimization could be performed, we only considered the ENZ nanoparticle with radii $a_{2,1} = \{98, 100\}$ nm, as it shows the capabilities of our approach shown in Fig. 3 and corresponds to experimentally plausible nanoparticles [34].

In addition, we numerically calculated the fundamental extinction cross sections and the ENZ-dependent parametric
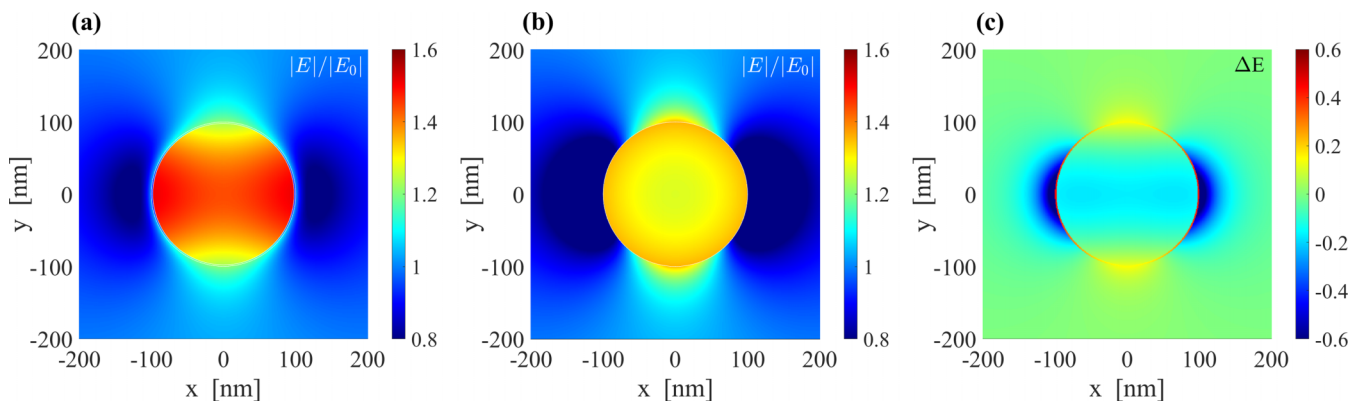

FIG. 3. Electric field for the bilayer structure, $a_{2,1} = \{98, 100\}$ nm at the ENZ wavelength. (a) Actual bilayer structure. (b) Bulk effective-medium structure. (c) Difference of the normalized near-field distribution between (b) and (a). As can be seen from (c), the two simulations are in good agreement with each other in general and they differ only in the vicinity of the surface.
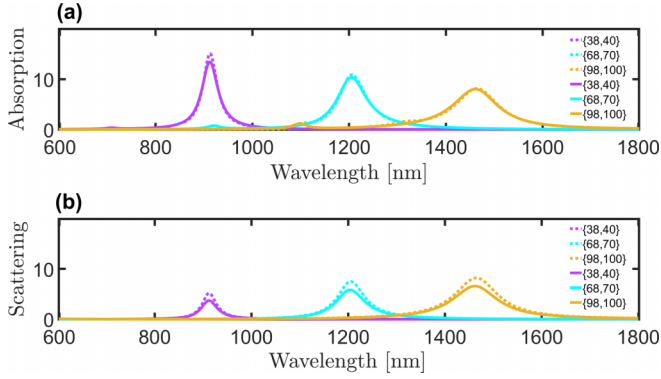
FIG. 4. (a) Absorption and (b) scattering cross sections for the bilayered spherical nanoparticles with full permittivity (solid lines) and effective permittivity (dashed lines) for radii $a_{2,1} = \{38, 40\}$ nm, $a_{2,1} = \{68, 70\}$ nm, and $a_{2,1} = \{98, 100\}$ nm. The values in the legend represent the radius values of the inner and outer spherical layers.

sweep for different layers of the ENZ nanoparticle in the case of a plane wave incident on it using full permittivity (without any effective-medium approximation) and the effective permittivity, coming from the effective-medium formulation. Figures 4(a) and 4(b) show the calculated absorption and scattering cross sections for three different ENZ nanoparticles using STRATIFY, i.e., $a_{2,1} = \{38, 40\}$ nm (purple), $a_{2,1} = \{68, 70\}$ nm (cyan), and $a_{2,1} = \{98, 100\}$ nm (orange), with absorption and scattering peak resonances at $\lambda \approx 913, 1206,$ and 1466 nm, respectively. The maximum extinction resonance wavelengths for the proposed ENZ nanoparticles are redshifted compared to their characteristic ENZ wavelengths, which are presented in Table I. This is due to the resonant excitation of dipole surface plasmons on the ENZ nanoparticle. We note in fact that the obtained resonance enhancement for both scattering and absorption cross sections occurs when the condition $\varepsilon_{\text{eff}} \approx -2$ (the so-called Fröhlich condition) for spherical nanoparticles is satisfied [35]. The absorption and scattering for the ENZ nanoparticle $a_{2,1} = \{98, 100\}$ nm have appreciably similar peak values. However, for the ENZ nanoparticle $a_{2,1} = \{38, 40\}$ nm and $a_{2,1} = \{68, 70\}$ nm, we obtain relatively low scattering peak values compared to its corresponding absorption cross-section peak values. It is also interesting to note that by changing the filling ratio of the ENZ nanoparticle, a passive tuning of the λ_{ENZ} can be observed, which corroborates the shift in the nanoparticle's peak absorbance and scattering cross sections. Intuitively, the redshift of the peak in the dipole resonance with increasing size could be linked to the weakening of their restoring force. Since the distance between charges on opposite sides of the ENZ

TABLE I. The ENZ nanoparticles with their characteristic ENZ wavelengths as well as their corresponding resonance wavelengths.

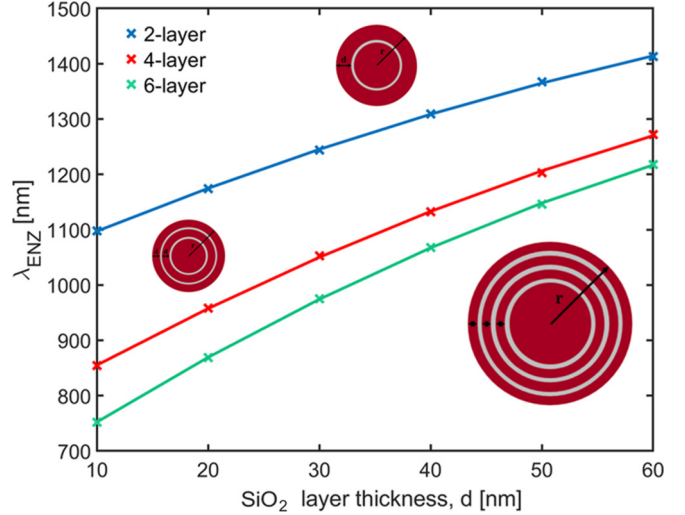| Nanoparticle size (nm)	λ_{ENZ} (nm)	$\lambda_{\text{resonance}}$ (nm)
{38, 40}	659	913
{68, 70}	852	1206
{98, 100}	1010	1466

FIG. 5. The ENZ wavelengths calculated for three different structures of a set of SiO$_2$ layers, with varying thicknesses d. The SiO$_2$ inner core and the Ag layers in between are fixed with a radius of $a_2 = \{98\}$ nm and a thickness of 2 nm. The compositions of the multilayer nanospheres are schematically presented with red (SiO$_2$) and gray (Ag) circular layers, next to the relevant λ_{ENZ} plots, corresponding to two (blue), four (red), and six layers (green), with thickness d values ranging from 10 to 60 nm.

nanoparticle increases with size, in fact, their corresponding interaction decrease.

In addition to the absorption and scattering cross section of the ENZ nanoparticles, we numerically calculated the ENZ wavelengths for different layered nanoparticles by parametrically varying the thickness of SiO$_2$ overlaid on the outer Ag shell. The SiO$_2$ inner core and the Ag layers in between are fixed with a radius of $a_2 = \{98\}$ nm and a thickness of 2 nm. It is evident in Fig. 5 that by changing the thicknesses of the embedded SiO$_2$ layers, we attain different ENZ wavelengths for the other multilayered nanoparticles. For all the considered nanostructures, we see a linear trend that depicts that by varying the thicknesses of the SiO$_2$ layers, there is a corresponding shift in λ_{ENZ} for different layered structures. This signifies the possibility of extending the effective-medium formulation of the bilayered structure into multilayered nanoparticles.

V. CONCLUSION

Our work showed that effective-medium theory is potentially applicable to bilayer spherical nanoparticles to determine their unique spectral responses and ENZ properties. By changing the diameter of the ENZ nanoparticle, we identified a spectral shift in the spectral absorbance and scattering cross sections of the ENZ nanoparticle, which signifies a passive tuning of the proposed structure. As shown in subsequent discussion, the effective permittivity formulation works relatively well for bilayer structures and could be easily extended to multilayered structures. Although in this work we have only considered Ag-SiO$_2$ nanoparticles, as they are the most common and readily available commercially, our approach can in principle be applied to any combination of metal-dielectric material that follows the prescriptions we have given above.

However, the condition $a_1 \leqslant \lambda_{\mathrm{ENZ}}/10$ is specific to Ag-SiO$_2$ and will take a different form, once the metal and/or dielectric is changed. Furthermore, as each metal's dispersion is different, this may change the spectrum as well as the ENZ wavelength. One can use different thicknesses and dielectric materials to adjust the wavelength and spectrum when the material is different. The electric-near-field response for both the bilayer and the effective-medium structures shows similar near-field optical responses. Our proposed ENZ nanoparticle can be obtained by low-cost chemical synthesis techniques to be utilized in applications that grasp the advantage of ENZ properties as well nanoparticle properties.

[1] A. Alù, M. G. Silveirinha, A. Salandrino, and N. Engheta, Epsilon-near-zero metamaterials and electromagnetic sources: Tailoring the radiation phase pattern, Phys. Rev. B **75**, 155410 (2007).

[2] J. Zheng, H. A. Almossalami, K. Chen, X. Yu, and H. Ye, Permittivity acquisition of plasmonic materials at epsilon near zero wavelengths, J. Appl. Phys. **129**, 103101 (2021).

[3] G. V. Naik, J. Kim, and A. Boltasseva, Oxides and nitrides as alternative plasmonic materials in the optical range [invited], Opt. Mater. Express **1**, 1090 (2011).

[4] J. Gao, L. Sun, H. Deng, C. J. Mathai, S. Gangopadhyay, and X. Yang, Experimental realization of epsilon-near-zero metamaterial slabs with metal-dielectric multilayers, Appl. Phys. Lett. **103**, 051111 (2013).

[5] R. Maas, J. Parsons, N. Engheta, and A. Polman, Experimental realization of an epsilon-near-zero metamaterial at visible wavelengths, Nat. Photon. **7**, 907 (2013).

[6] M. Habib, I. Issah, E. Bermúdez-Ureña, and H. Caglayan, Self-rolling SiO$_2$/Au based epsilon-near-zero metamaterials, Adv. Opt. Mater. **10**, 2200081 (2022).

[7] E. J. R. Vesseur, T. Coenen, H. Caglayan, N. Engheta, and A. Polman, Experimental Verification of $n = 0$ Structures for Visible Light, Phys. Rev. Lett. **110**, 013902 (2013).

[8] U. Guler, V. M. Shalaev, and A. Boltasseva, Nanoparticle plasmonics: Going practical with transition metal nitrides, Mater. Today **18**, 227 (2015).

[9] J. Yang, H. A. Almossalami, Z. Wang, K. Wu, C. Wang, K. Sun, Y. M. Yang, and H. Ye, Direct observations of surface plasmon polaritons in highly conductive organic thin film, ACS Appl. Mater. Interfaces **11**, 39132 (2019).

[10] C. Graf and A. Van Blaaderen, Metallodielectric colloidal core-shell particles for photonic applications, Langmuir **18**, 524 (2002).

[11] K. Hasegawa, C. Rohde, and M. Deutsch, Enhanced surface-plasmon resonance absorption in metal-dielectric-metal layered microspheres, Opt. Lett. **31**, 1136 (2006).

[12] S. A. Scherbak and A. A. Lipovskii, Understanding the second-harmonic generation enhancement and behavior in metal core-dielectric shell nanoparticles, J. Phys. Chem. C **122**, 15635 (2018).

[13] Y. Pu, R. Grange, C. L. Hsieh, and D. Psaltis, Nonlinear Optical Properties of Core-Shell Nanocavities for Enhanced Second-Harmonic Generation, Phys. Rev. Lett. **104**, 207402 (2010).

[14] M. A. Ochsenkühn, P. R. Jess, H. Stoquert, K. Dholakia, and C. J. Campbell, Nanoshells for surface-enhanced Raman spectroscopy in eukaryotic cells: Cellular response and sensor development, ACS Nano **3**, 3613 (2009).

[15] P. K. Jain and M. A. El-Sayed, Surface plasmon resonance sensitivity of metal nanostructures: Physical basis and universal scaling in metal nanoshells, J. Phys. Chem. C **111**, 17451 (2007).

[16] C. Zhang, T. Zhang, Z. Zhang, and H. Zheng, Plasmon enhanced fluorescence and Raman scattering by [Au-Ag alloy NP cluster]@SiO$_2$ core-shell nanostructure, Front. Chem. **7**, 647 (2019).

[17] C. K. Chan, R. C. Flagan, and J. H. Seinfeld, Resonance structures in elastic and Raman scattering from microspheres, Appl. Opt. **30**, 459 (1991).

[18] F. Zhang, G. B. Braun, Y. Shi, Y. Zhang, X. Sun, N. O. Reich, D. Zhao, and G. Stucky, Fabrication of Ag@SiO$_2$@Y$_2$O$_3$:Er nanostructures for bioimaging: Tuning of the upconversion fluorescence with silver nanoparticles, J. Am. Chem. Soc. **132**, 2850 (2010).

[19] V. S. Zuev, SPASER laser and Purcell factor, Opt. Spectrosc. **109**, 760 (2010).

[20] M. A. Noginov, G. Zhu, A. M. Belgrave, R. Bakker, V. M. Shalaev, E. E. Narimanov, S. Stout, E. Herz, T. Suteewong, and U. Wiesner, Demonstration of a spaser-based nanolaser, Nature (London) **460**, 1110 (2009).

[21] I. S. Curtis, R. J. Wills, and M. Dasog, Photocatalytic hydrogen generation using mesoporous silicon nanoparticles: Influence of magnesiothermic reduction conditions and nanoparticle aging on the catalytic activity, Nanoscale **13**, 2685 (2021).

[22] D. Rativa and L. A. Gómez-Malagón, Colloidal plasmonic structures for harvesting solar radiation, Renewable Energy **118**, 947 (2018).

[23] A. D. Phan, N. B. Le, N. T. Lien, and K. Wakabayashi, Multilayered plasmonic nanostructures for solar energy harvesting, J. Phys. Chem. C **122**, 19801 (2018).

[24] M. G. Blaber, M. D. Arnold, and M. J. Ford, A review of the optical properties of alloys and intermetallics for plasmonics, J. Phys.: Condens. Matter **22**, 143201 (2010).

[25] I. L. Rasskazov, P. S. Carney, and A. Moroz, STRATIFY: A comprehensive and versatile MATLAB code for a multilayered sphere, OSA Continuum **3**, 2290 (2020).

[26] P. B. Johnson and R. W. Christy, Optical constants of the noble metals, Phys. Rev. B **6**, 4370 (1972).

[27] L. F. Chen, C. K. Ong, and B. T. G. Tan, Effective permittivity of layered dielectric sphere composites, J. Mater. Sci. **33**, 5891 (1998).

[28] C. T. Tai, *Dyadic Green's Function in Electromagnetic Theory* (The Book Service, Colchester, 1972).

[29] W. C. Chew, *Waves and Fields in Inhomogeneous Media* (Kluwer, Amsterdam, 1990).

[30] G. T. Papadakis, P. Yeh, and H. A. Atwater, Retrieval of material parameters for uniaxial metamaterials, Phys. Rev. B **91**, 155406 (2015).

[31] P. Shekhar, J. Atkinson, and Z. Jacob, Hyperbolic metamaterials: fundamentals and applications, Nano Convergence **1**, 14 (2014).

[32] J. D. Jackson, *Classical Electrodynamics*, 2nd ed. (Wiley, New York, 1975).

[33] Y. Guo, C. L. Cortes, S. Molesky, and Z. Jacob, Broadband super-Planckian thermal emission from hyperbolic metamaterials, Appl. Phys. Lett. **101**, 131106 (2012).

[34] X. Zhang, S. Ye, X. Zhang, and L. Wu, Optical properties of SiO_2@M (M = Au, Pd, Pt) core-shell nanoparticles: Material dependence and damping mechanisms, J. Mater. Chem. C **3**, 2282 (2015).

[35] X. Fan, W. Zheng, and D. J. Singh, Light scattering and surface plasmons on small spherical particles, Light Sci. Appl. **3**, e179 (2014).